Inorganic Chemistry

Article

pubs.acs.org/IC

Selective Synthesis of Cu_2O and Cu/Cu_2O NPs: Antifungal Activity to Yeast *Saccharomyces cerevisiae* and DNA Interaction

K. Giannousi,[†] G. Sarafidis,[†] S. Mourdikoudis,[§] A. Pantazaki,[‡] and C. Dendrinou-Samara*[,†]

[†]Laboratory of Inorganic Chemistry and [‡]Laboratory of Biochemistry, Department of Chemistry, Aristotle University of Thessaloniki, 54124 Thessaloniki, Greece

[§]Departamento de Química Física, Universidade de Vigo, 36310 Vigo, Spain

ABSTRACT: A facile selective synthesis of Cu_2O and heterogeneous Cu/Cu_2O nanoparticles (NPs) was achieved through a solvothermal approach by $Cu(NO_3)_2$ in proportion of three different surfactants, namely, tetraethylene glycol (TEG), oleylamine (OAm) and polyoxyethylene (20) sorbitan laurate (Tween 20). Formation aspects for the spherical Cu_2O@OAm (30 nm) and Cu_2O@Tween (12 nm) as well as for the core−shell and semishell Cu/Cu_2O@TEG NPs (7 nm) and the Cu/Cu_2O@OAm (170 nm) nanorods have been proposed. The fungistatic and fungicidal activity of the newly synthesized NPs was studied *in vitro* against the yeast *Saccharomyces cerevisiae*, which constitutes a unicellular eukaryotic model microorganism in molecular and cell biology.

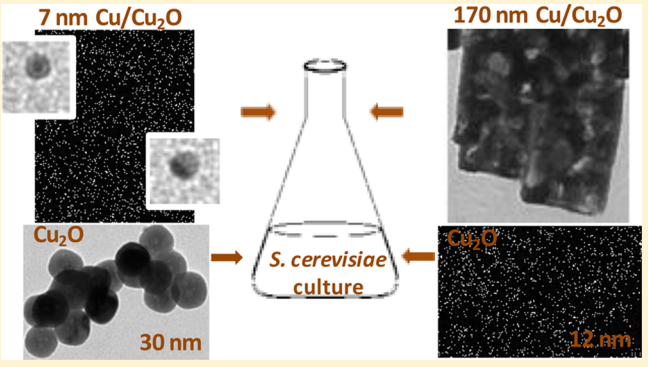

The antifungal results, based on optical density and fluorescence measurements, clearly indicate that the composition, size, and amount of surfactant are of key importance in the antifungal properties of the NPs. Cu_2O@OAm NPs exhibited the most prominent antifungal activity with 3.73 μg/mL $IC_{50viability}$ value. The isolated DNA of *S. cerevisiae* cells after exposure to the NPs was investigated, and binding and/or degradation phenomena were recorded that are correlated to the size and concentration of the NPs. Their activity pathway was further explored, and reactive oxygen species production and lipid peroxidation were verified mainly for Cu_2O NPs.

1. INTRODUCTION

Nowadays, microbial resistance to the widely used antibiotics has increased rapidly, and as far as antifungal therapy is concerned, there is an urgent need for antibiotics with novel antimicrobial mechanisms, since fungi are eukaryotic organisms with structures and metabolisms that are similar to those of eukaryotic hosts.[1,2] Recently, inorganic metal oxides, for example, MgO, ZnO, and TiO_2, are increasingly used as antimicrobials owing to their stability and long shelf life compared with the organic antimicrobial agents.[3] Exploration of nanostructures offers new possibilities in biological context, since when the particle size decreases the surface area increases resulting in enhanced biological activity per given mass compared to larger particles.[4]

Metallic copper as well as cupric oxide (CuO) or cuprous oxide (Cu_2O) nanoparticles, named as copper-based nanoparticles (Cu-based NPs), have attracted attention from diverse disciplines due to the widespread use in electronics, optics, sensors, catalysts, and medical applications.[5] The antimicrobial activity of copper has long been recognized.[6] However, relatively few studies have been focused on the antimicrobial properties of Cu-based NPs, and as a result there is still a lack of definite knowledge regarding their mechanism of action. An elusive question remains whether the release of copper ions from the crystalline core of copper nanoparticles contributes to the toxicity of these nanomaterials or the toxicity exerts from the nanoparticle itself.[7] Specifically, relatively big (60−80 nm) Cu NPs[8,9] as well as CuO NPs of sizes within a range of 8−40 nm[10−13] or Cu_2O NPs of micron sizes[14−16] were found with enhanced antibacterial properties and specificity against Gram-positive and Gram-negative bacterial strains. Meanwhile, the antifungal effect has received only marginal attention, and to our knowledge a small number of reports have been published;[17,18] Cu NPs of 9−34 nm and nanorods (NRs) of width 21 nm have been tested against *Stachybotrys chartarum*, and relatively low minimum inhibitory concentration (MIC) values (<25 μg/mL) have been recorded,[17] while spherical Cu NPs (5−10 nm) have been tested against plant pathogenic fungi *Phoma destructive*, *Curvularia lunata*, *Alternaria alternata*, and *Fusarium oxysporum* and showed promising antifungal activity.[18] The activity of CuO NPs (30 nm) has also been studied toward the yeast *Saccharomyces cerevisiae* from a toxicity point of view, and the results demonstrated relative resistance compared with other unicellular microorganisms (bacteria and algae).[19] Nevertheless, the reaction pathway has not been explored.

Received: May 16, 2014
Published: September 4, 2014

Additionally, the synthesis of stable and low polydispersity Cu-based NPs remains an interesting task mainly because of the rapid air oxidation of metallic copper to Cu^{2+} ions and/or Cu_xO oxides (x = 1 or 2)[17] in addition with the unique properties of the nanosizes. A number of different synthetic approaches have been proposed, as it is widely accepted that the composition, size, and shape of the NPs can be tuned by controlling the reaction conditions such as time, temperature, pH, and the concentration of reagents as well as of surfactants.

Herein, we continued our efforts toward the synthesis of Cu-based NPs as antifungal and antimicrobial agents.[20,21] In the present study we utilized polysorbate 20 (Tween 20), tetraethylene glycol (TEG), and oleylamine (OAm) in a solvothermal approach to synthesize Cu_2O NPs and heterogeneous Cu/Cu_2O NPs and nanorods (NRs) in a controlled manner upon adjusting the reaction time and temperature. The study of their *in vitro* fungistatic and fungicidal activity against the yeast *S. cerevisiae* was carried out. *S. cerevisiae* was chosen as it constitutes a unicellular eukaryotic model microorganism in molecular and cell biology.[22] The interaction with DNA isolated from the exposed fungal cells, by means of binding and/or degradation, was also investigated. Furthermore, their activity pathway was explored in terms of oxygen ion (O_2^-) production and lipid peroxidation, since Cu-based NPs can produce reactive oxygen species (ROS), which disrupt the cell wall and membrane integrity as well as damage cellular lipids, carbohydrates, and DNA.[7,19,20]

2. EXPERIMENTAL SECTION

2.1. Materials. Copper(II) nitrate trihydrate $Cu(NO_3)_2{\cdot}3H_2O$ (Merck, ≥99.5%, M = 241.60 g/mol), hydrazine hydrate $N_2H_4{\cdot}H_2O$ (Merck, ∼100%, M = 50.06 g/mol), tetraethylene glycol (TEG) (Sigma-Aldrich, 99%, M = 194.23 g/mol), oleylamine (OAm) (Sigma-Aldrich, 70%, M = 267.49 g/mol), and polyoxyethylene (20) sorbitan laurate (Tween 20) (TCI, >97%, M = 1200 g/mol) were of analytical grade and were used without any further purification. Agarose (BRL), Tryptone, yeast extract (Oxoid, Unipath Ltd., Hampshire, UK). Intercalative dye ethidium bromide (Eth-Br) (Sigma), nitroblue tetrazolium (NBT) (Sigma), thiobarbituric acid (TBA) (Sigma), RNase A (Sigma), proteinase K (Sigma), fluorescein diacetate (FDA, 3,6-diacetoxyfluoran) (Sigma).

2.2. Preparation of Cu-based NPs. Cu-based NPs were prepared solvothermally where time duration and temperature were selected for the desired composition and size and were based on our previous results.[20,21] Concerning sample S1, 4.13 mmol (1 g) $Cu(NO_3)_2{\cdot}3H_2O$ were dissolved in 4 mL of deionized water to obtain a blue solution. Then 4.13 mmol (0.207 g) of hydrazine $N_2H_4{\cdot}H_2O$ and 58 mmol (10 mL) of TEG were added. The resulting brownish mixture was transferred into a 23 mL Teflon-lined stainless-steel autoclave. The crystallization was carried out under autogenous pressure at 120 °C for 2 h. For sample S2, 4.13 mmol of $Cu(NO_3)_2{\cdot}3H_2O$ were dissolved in 10 mL of OAm. The dark blue-colored resulting mixture was transferred into a Teflon-lined stainless steel autoclave, and the reaction was allowed to continue for 24 h at 200 °C. In the case of sample S3, 4.13 mmol of $Cu(NO_3)_2{\cdot}3H_2O$ were dissolved in 4 mL of deionized water to obtain a blue solution, while 4.13 mmol (0.207 g) of hydrazine $N_2H_4{\cdot}H_2O$ and 6 mL of OAm were added, resulting in a mucky brownish jelly. Again the crystallization was carried out under autogenous pressure at 200 °C for 24 h. Finally, sample S4 was prepared by adding 4.13 mmol (0.207 g) of hydrazine $N_2H_4{\cdot}H_2O$ and 4.1 mmol (5 g) of Tween 20 to the copper nitrate solution (4.13 mmol $Cu(NO_3)_2{\cdot}3H_2O$ dissolved in 10 mL of deionized water), while the temperature was adjusted at 140 °C for 4 h. Afterward in all cases (samples S1−S4), the autoclave was cooled naturally to room temperature, and after centrifugation at 5000 rpm, the supernatant liquids were discarded; the precipitates were obtained and washed with ethanol, at least three times, to remove the excess ligands and unreacted agents.

2.3. NPs Characterization. X-ray powder diffraction (XRD) measurements were performed on a Philips PW 1820 diffractometer at a scanning rate of 0.050/3 s, in the 2θ range from 10 to 90°, with monochromatized Cu Kα radiation (λ = 1.5406 nm). Transmission electron microscopy (TEM) images were obtained with a JEOL JEM 1010 microscope (TEM), operating at an acceleration voltage of 100 kV. For TEM observations we have used suspensions of the NPs deposited onto Formvar/carbon coated copper grids. Thermogravimetric (TG) analysis (SETA-RAM SetSys-1200) was carried out in the range from room temperature to 900 °C at a heating rate of 10 °C min^{-1} under N_2 atmosphere. Infrared spectra (280−4000 cm^{-1}) were recorded on a Nicolet FTIR 6700 spectrometer with samples prepared as KBr pellets. The micro-Raman measurements were performed at room temperature using the 514.6 nm line of an Ar ion laser as the excitation source. The power was kept at 0.1 mW, and a 100 μm lens was used. The spectra were recorded using a micro-Raman Dilor XY triple monochromator coupled to a charge-coupled device (CCD) detector. All the fluorescence spectra were recorded by a Hitachi F7000 fluorescence spectrophotometer. The excitation wavelength for all samples was 455 nm giving an emission maximum at approximately 515 nm.

2.4. Antifungal Activity Studies. *2.4.1. Culture Media.* The cultivation medium used for antifungal activity test was the minimal medium salts broth (MMS). It contains 1.5% (w/v) glucose, 0.5% (w/v) NH_4Cl, 0.5% (w/v) K_2HPO_4, 0.1% (w/v) NaCl, 0.01% (w/v) $MgSO_4{\cdot}7H_2O$, and 0.1% (w/v) yeast extract. The pH of the medium was adjusted to 7.0.

2.4.2. Screening of the NPs for Antifungal Activity. The yeast *S. cerevisiae* was used as a model organism to screen the antifungal properties of the newly prepared NPs. A series of different cultures were prepared, while each of them consists of 20 mL of MMS inoculated with 3 mg of yeast *S. cerevisiae*. Subsequently, the precultures grown at the optimal growth temperature (30 °C) until the middle of exponential phase were separated in 2 mL aliquots. In a first group of aliquots, various concentrations of NPs were added to reach a final concentration of 2.5, 5, 10, 25, 50, and 100 μg/mL of the NPs, respectively. The stock solutions of the NPs (2.5 mg/mL) were prepared by dissolving in distilled water. A second group of the same cultures, supplemented with the suitable concentrations of the NPs, was tested, but it was devoid of inoculums. These cultures were prepared to monitor any possible presence of fungus or micro-organisms able to grow in this medium. A third group of cultures, supplemented with inoculum but devoid of NPs, was used, which indicated the fungal growth profile in the absence of NPs (cultures of reference). All cultures were incubated at 30 °C for 22 h. Fungal growth was measured as increase in absorbance at 600 nm determined using a spectrophotometer (Thermo Electron Corporation, Helios γ, USA). The absorbance values for the cultures of reference were considered as 100% of growth to calculate the percentage of growth inhibition of yeast *S. cerevisiae* resulting from the presence of NPs. The MIC in μg/mL, defined as the lowest concentration of a compound or material that inhibits 50% of the growth (IC_{50} value) of an organism,[23] was determined based on inhibition growth of batch cultures, containing varying concentrations of the NPs in suspension.[24,25]

2.4.2.1. Fungus Viability. The fungus viability in the absence and the presence of various concentrations of NPs was also estimated by determining the degree of enzymatic hydrolysis of fluorescein diacetate (FDA, 3,6-diacetoxyfluoran) by *S. cerevisiae* cultures. In detail, FDA is cleaved to fluorescein and acetic acid by different enzymes, such as proteases, lipases, and esterases. These enzymes are constituents of the primary metabolism of fungus and micro-organisms.[26] The released fluorescein was measured by a fluorescence spectrophotometer.

A stock solution of fluorescein diacetate in acetone (2 mg/mL) was added to reach a final FDA concentration of 10 $\mu g/mL^{-1}$ in two series of *S. cerevisiae* cultures grown until the middle of exponential phase in the absence and presence of various concentrations of NPs. These cultures were incubated at room temperature on a rotary shaker (120 rpm) for 1 h in total. After intervals of 15 min, 1 mL aliquots were

dx.doi.org/10.1021/ic501143z | Inorg. Chem. 2014, 53, 9657−9666

taken from the aliquots and placed in eppendorf tubes. The hydrolysis of FDA was terminated by addition of acetone to reach a final acetone concentration of 50% v/v.[26] The mixture was centrifuged for 5 min in a multipurpose centrifuge (ScanSpeed 1236MG, LaboGene) at 10 000 rpm to remove suspended particles, and finally the fluorescence was measured.

2.4.3. S. cerevisiae Genomic DNA Isolation. *S. cerevisiae* cells from 5 mL of the overnight cultures were washed several times with phosphate-buffered saline and were pelleted in a microcentrifuge tube. The cell pellets were resuspended in 200 μL of lysis buffer [2% Triton X-100, 1% SDS, 100 mM NaCl, 10 mM Tris-HCl (pH 8.0), 1 mM EDTA (pH 8.0)]. The tubes were placed on ice for 2 min (until they were completely frozen), then immersed in a 95 °C water bath for 1 min to thaw quickly, and finally were vortexed vigorously for 30 s. The process was repeated twice.[27] After centrifugation for 5 min at 1600*g* the supernatants are collected, brought to 1% SDS, and treated for 2 h with RNase A (final concentration 5 μg/mL) at 56 °C followed by digestion with proteinase K (final concentration of 2.5 μg/mL) for at least 2 h at 37 °C. After addition of 1/2 vol of 10 M ammonium acetate, the DNA is precipitated with 2.5 vol of ethanol.[28]

2.4.4. Fungal DNA Binding/Cleavage Experiment in Agarose Gel Electrophoresis. The DNA binding/cleavage efficiency of the NPs was measured by determining their ability to alter the mobility of the fungal DNA bands and/or to cause degradation. Reactions, which contained aliquots of 3 μg of nucleic acid, were incubated at a constant temperature of 30 °C for 24 h in the presence of various concentrations of NPs in a buffer A to a final volume of 20 μL. It was terminated by the addition of 5 μL of loading buffer consisting of 0.25% w/v bromophenol blue and 30% v/v glycerol in water. The products resulting from interactions of the NPs with DNA were separated by electrophoresis on agarose gels (1% w/v), which contained 1 μg/mL ethidium bromide in 40×10^{-3} M Tris−acetate, pH 7.5, 2×10^{-2} M sodium acetate, 2×10^{-3} M Na_2EDTA, at 5 V·cm^{-1}. Agarose gel electrophoresis was performed in a horizontal gel apparatus (Mini-SubTM DNA Cell, BioRad) for about 1 h. The gels were visualized after staining with the fluorescence intercalated dye ethidium bromide under a UV illuminator.

2.4.5. Reactive Oxygen Species Assay. The reactive oxygen species (ROS), which are created intracellularly as result of treatment of *S. cerevisiae* with the NPs, were measured by the nitroblue tetrazolium (NBT) reduction using the protocol described by Becerra et al.[29] For this purpose 100 μL of fungal suspension (where OD_{600} = 1.5) in MMS was incubated with respective NPs (samples S1−S4) and 500 μL of 1 mg/mL NBT for 1 h at 30 °C. Then, 100 μL of 0.1 M HCl was added, and the tubes were centrifuged at 1500*g* for 10 min. The pellets were treated with 600 μL of dimethyl sulfoxide to extract the reduced NBT. Finally, 500 μL of MMS was added, and formazan blue obtained from cells was measured as optical density (OD) at 575 nm (intracellular ROS).

2.4.6. Lipid Peroxidation Measurement. *S. cerevisiae* cells were initially cultivated on lysogeny broth medium for 24 h at 30 °C and then were collected when culture reached exponential or stationary phase. Cells were suspended in buffer A, and aliquots containing 50 mg of cells were in each tube. Fungal cells in exponential phase (50 mg) were directly exposed to increasing concentrations of NPs (samples S1−S4) for 1 h at 30 °C. Then cells were harvested by centrifugation and washed twice with distilled water. The pellets were resuspended in 500 μL of 10% trichloroacetic acid (TCA) and transferred to a tube containing 1.5 g of glass beads. Cells were lysed by 15 cycles of agitation in a vortex for 20 s and incubated on ice for 20 s, followed by 30 cycles of sonication at 225 W for 10 s and 10 s incubation on ice. The supernatants obtained after centrifugation were mixed with 0.1 mL of 0.1 M EDTA and 0.6 mL of 0.1% w/v thiobarbituric acid in 0.05 M NaOH. The reaction mixture was incubated at 100 °C for 15 min. The samples were cooled and centrifuged (5900 g for 5 min), and the appearance of malondialdehyde (MDA) was recorded by measuring in the supernatant the absorbance at 532 nm and compared to a standard curve containing 0−3.2 μM malondialdehyde.[30]

3. RESULTS AND DISCUSSION

In an attempt to evaluate the efficacy of Cu_2O NPs and heterogeneous Cu/Cu_2O NPs for potential use as antifungal agents, the solvothermal procedure as a simple and eco-friendly method was chosen. The reaction conditions due to the closed system are easily reproducible and can be further scaled up for mass production. Because of the ability of copper ions to easily interconvert between Cu(I)/Cu(II) by Fenton-like and Haber−Weiss reactions,[23] preparation of stable Cu_2O NPs is of particular interest. Three different biocompatible and nonionic surfactants/capping agents, namely, TEG, OAm, and Tween 20, were selected. Surfactants constitute unique reaction media and appear to play the key factor in the morphology of the NPs, since they not only protect them from agglomeration but also drive their formation. Meanwhile, the antifungal activity is affected by the surface charge of NPs, as the toxicity effect toward microbes is reduced when charge is decreased;[31] thus, neutral surfactants are required. Moreover, the mild reducing ability of TEG as polyalcohol (sample S1) and OAm as a long-chain alkylamine (samples S2 and S3) were considered to be advantageous for the desired compositions. In addition, as the mixed potential decreases with the increase both in pH and temperature,[32] hydrazine was used as an extra reducing agent, and temperature was elevated in proportion of the solvent in each case. For sample S4, where Tween 20 was implemented, the adjusted reaction conditions were based on our previous findings.[20,21] The newly synthesized Cu-based NPs were well-characterized, as it is widely accepted that the intrinsic characteristics of the NPs affect the microorganisms and their biological activity.

3.1. Characterization of NPs. The XRD patterns of samples S3 and S4 (Figure 1) exhibit Bragg reflections that

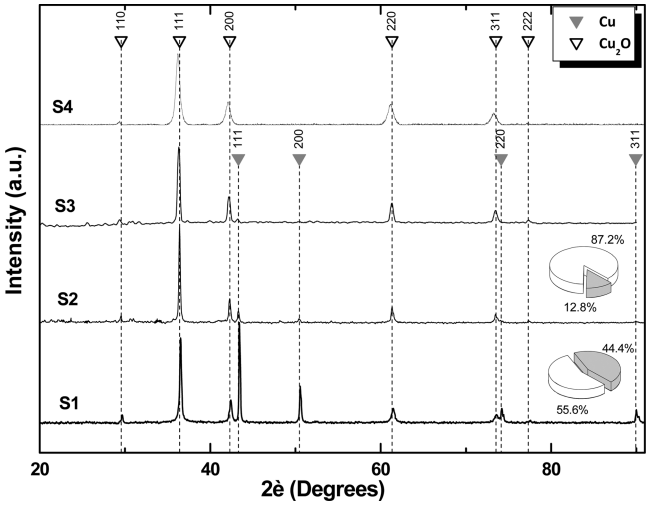

Figure 1. XRD patterns of samples S1, S2, S3, and S4. Vertical lines denote expected diffraction peak positions for Cu_2O (▽) and Cu (▼). (inset) The phase ratio of samples S1 and S2.

correspond to the crystal structure of Cu_2O, while in the case of samples S1 and S2 two phases coexist, ascribed to face-centered cubic (*fcc*) copper (JCPDS Card No. 04−0836) and to the cubic ($Pn3m$) crystal structure of Cu_2O (JCPDS Card No. 05−0667) (Figure 1). The average crystalline sizes of pure Cu_2O NPs (S3 and S4), determined by taking the full width at half-maximum (fwhm) of the most intense peak and by using the Scherrer equation, were found to be 33 and 15 nm, respectively.

dx.doi.org/10.1021/ic501143z | Inorg. Chem. 2014, 53, 9657−9666

By using MDI's Jade software, lattice parameters were calculated and were found to be a = 4.28 Å (S3) and 4.29 Å (S4), while the same value of 4.26 Å received for the Cu_2O phase of S1 and S2, very close to the theoretical bulk values of Cu_2O (a = 4.27 Å). The lattice parameters of Cu phase of S1 and S2 were found 3.61 Å identical to bulk Cu (a = 3.61 Å). These results, in proportion with the sharp features, reveal the high crystalline structure of the samples. The phase ratio for the Cu/Cu_2O NPs (samples S1 and S2) was also calculated by MDI's Jade software as given in Figure 1 inset.

TEM micrographs of all samples (S1−S4) prepared in the presence of different surfactants are illustrated in Figure 2.

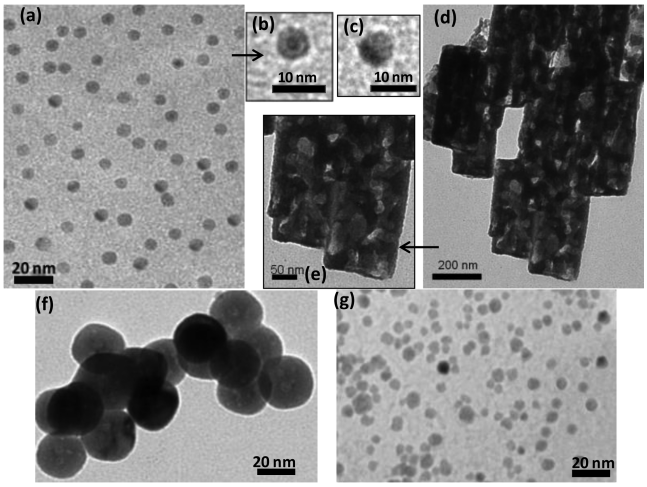

Figure 2. TEM images of samples S1 (a), S2 (d), S3 (f), and S4 (g). Low-magnification TEM images of sample S1: one single core−shell NP (b), semishell NP (c), and surface-oxidized nanorods with many oxide pits of sample S2 (e).

When we used TEG as surfactant (S1) spherical NPs of approximately 7 nm were formed (Figure 2a), while the contrast is not uniform; some domains of the NPs appear lighter than others, indicating that oxidation process took place. On the basis of the higher percentage of Cu_2O in the sample compared to Cu, we assume that Cu_2O shell was formed from sacrificing the copper core, resulting in the formation of core−shell NPs (Figure 2b) or semishell NPs (Figure 2c).[33] In the case of using OAm in double role of surfactant and reducing agent, heterogeneous Cu/Cu_2O NRs of 170 nm width (S2) were isolated (Figure 1d). The oxide pits observed with a higher magnification along the nanorods (Figure 1e) indicate the nonuniform surface oxidation on the nanostructure.[34] On the other hand, when a two-phase system OAm/water in the presence of extra reducing agent hydrazine (S3), pure Cu_2O NPs of 30 nm were formed (Figure 2f). Their shape was nearly spherical but with some defects, which appears like spots (light contrast) in their interior part. This hollowing process has also been demonstrated previously and is attributed to the gradual oxidation of the metallic core.[21,34] Concerning sample S4 prepared in the presence of Tween 20, the resulting nearly spherical Cu_2O NPs were significantly smaller (12 nm), and their morphology appears more uniform (Figure 2g) in comparison with the Cu_2O NPs prepared in the presence of OAm. The deviation found between the mean crystallite size from XRD and the particle size observed by TEM could be explained by taking into account that the Bragg peaks in XRD patterns are observed due to crystallinity of the sample. Hence, it is expected that a higher weight factor comes from larger crystallites.[35]

Table 1 summarizes characteristic FT-IR absorption bands of the samples S1−S4 corresponding to the functional groups of

Table 1. Characteristics FT-IR Absorption Bands of the Samples S1−S4

samples	IR (ν/cm^{-1}) (KBr pellet)
S1	$\nu_{(OH)}$: 1638; $\nu_{(C-O-C)}$: 1110
S2	$\nu_{(NH2)}$: 1554; $\nu_{(C=C)}$: 1635
S3	$\nu_{(NH2)}$: 1555; $\nu_{(C=C)}$: 1631
S4	$\nu_{asym(CO2)}$: 1628; $\nu_{sym(CO2)}$: 1381; $\nu_{(C-O-C)}$: 1100

the respective capping agents (Figure 3). In all cases the characteristic peaks found shifted compared to pure TEG (1646 cm^{-1}), OAm (1590 cm^{-1}), and Tween 20 (1110 cm^{-1}). For samples S2 and S3 (Figure 3b) the strong peak approximately at 1630 cm^{-1} present in both spectra is assigned to the double bond (δ(-C=C)) in the middle of OAm molecule with the intensity of this peak being characteristic of the bending configuration of OAm. In case of sample S4 (Figure 3c), the difference of asymmetric (ν_{as}) and symmetric (ν_s) stretching vibrations of laurate [$\Delta = \nu_{as}(CO_2) - \nu_s(CO_2)$] was found to be 247 cm^{-1}, indicating covalent binding.[36] In all samples the strong characteristic peak located at 625 cm^{-1} (shown in red circle) is assigned to the vibrations of Cu(I)−O bonds.[37]

Raman spectroscopy was used as an alternative tool to verify further the composition of the NPs (Figure 4). The presence of the crystalline Cu_2O was evidenced from the four distinct peaks displayed in all samples, while any other peaks attributed to different copper oxides are not detected.[38] The longitudinal optical phonon modes (LO) Γ_{12}^- at 109 cm^{-1} and the $\Gamma_{15}^{-(1)}$ at approximately 150 cm^{-1} are inactive Raman modes, while the most intense Raman signal is the second-order overtone 2 Γ_{12}^- (218 cm^{-1}).[39] Additionally, a broad peak with less intensity centered at approximately 630 cm^{-1} is observed, which corresponds to the red-allowed transverse phonon mode (TO)$\Gamma_{15}^{-(2)}$.[40] The lower intensity of the peaks (160−230 cm^{-1}) in case of S1 is correlated to the smallest percentage of Cu_2O phase compared to the other samples, corroborating further the XRD results.

The amount of residual surface capping agents of samples S1−S4 was evaluated by thermogravimetric analysis (TGA) over a temperature range as high as 900 °C under nitrogen atmosphere. The decomposition temperature of all pure surfactants is in the vicinity of 400 °C, while changes are attributed to the way of binding/adsorbing on the metal core. The cumulative organic content was estimated 17.5 wt % for TEG-capped NPs, 47.5 wt % for OAm-capped NRs, 25 wt % for OAm-capped NPs, and 28.9 wt % for Tween- capped NPs (Figure 5). Three weight losses were observed for TEG-capped NPs (S1), with the initial one being assigned to the loss of surface-adsorbed water. Considering the low amount of TEG the next two steps (~3.5% and ~9%, respectively) may be attributed to different kind of binding sites in agreement with a previous report.[41] The same thermal behavior was recorded in case of Tween 20-capped NPs (S4) with the first and the second weight loss (up to 300 °C) being attributed to water and CO_2 decomposition, respectively, while elimination of the laurate and the rest of the organic part followed at higher temperatures. However, for OAm-capped NPs, although similar

dx.doi.org/10.1021/ic501143z | Inorg. Chem. 2014, 53, 9657−9666

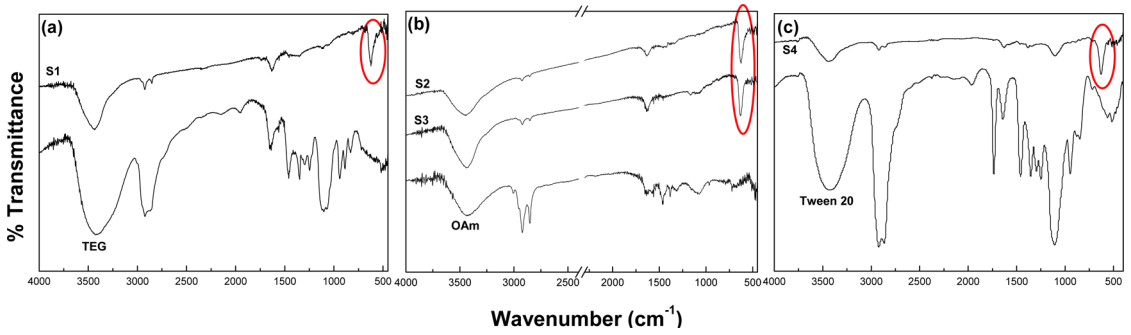

Figure 3. FTIR spectra of (a) TEG and sample S1, (b) OAm and samples S2 and S3, and (c) Tween 20 and sample S4.

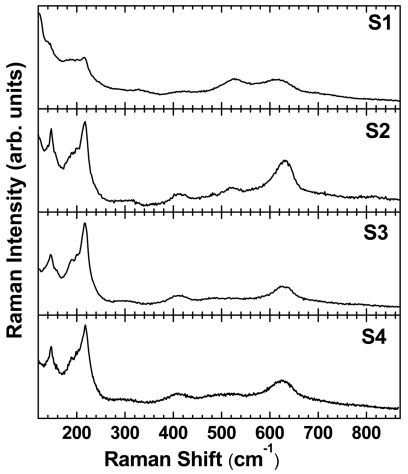

Figure 4. Raman spectra of samples S1−S4.

behavior of the two samples (S2 and S3) was found up to 300 °C, in the case of sample S2 an extra degradation step occurs up to 600 °C. Concerning decomposition in higher temperatures controversial explanations can be found in literature since double-stepped TGA curve is attributed to either a bilayer formation of the organic coating[42] or to two different kinds of binding sites.[41] Taking into account that the difference in the organic content between the two samples (S2 and S3) is opposed to the size of their metal core, since when surface area-to-volume ratio is increased a decrease of organic content is expected,[43] the extra region of mass reduction appeared only in this sample, can be ascribed to a double layer formation, arisen from the specific synthetic conditions, as this sample was prepared in pure OAm.

We tested the stability of the samples by recording XRD, IR, and Raman spectra, and there was no evidence of further oxidation for at least three months, indicating that the number of ligands coated on the surface of the NPs provide sufficient protection. To make a rough arithmetic estimation of the organic coating for the nearly spherical NPs (samples S1, S3, S4), we based on the presumptions that the density of the nanoparticles (6.1 g/cm^3) is the same for the above samples and that their shape is totally spherical.[44] As a result the number of ligands that are bound on the NPs was calculated (eq 1) and was found to be 1732, 6065, and 800 ligands per particle for S1, S3, and S4, respectively.

$$N = \frac{\omega N_A \rho \frac{4}{3}\pi R^3 \times 10^{-23}}{M} \quad (1)$$

where N is the number of ligands on each particle, R is the mean radius of the copper-based nanoparticles, ρ is the density of the NPs, N_A is Avogadro's number, M is the molar mass of surfactant molecules (g/mol), and ω is the mass loss in percent (%). From this formula, we also calculated the number of molecules per square centimeter ($\times 10^{14}$), which was 5.5, 8.58, and 1.76 for samples S1, S3, and S4, respectively. By comparing these values with those reported by R. De Palma et al.,[44] we can conclude that the ligands are densely packed on the surface of the NPs, which further justifies their improved stability.

3.2. Formation Aspects of Cu_2O and Cu/Cu_2O NPs. In general, the impact of temperature, time, pH and presence/absence of surfactant on the composition, size, and shape to the preparation of NPs is well-known. Plurality of the factors as well as Cu(I/II) flexible redox behavior through numerous of different synthetic methods make synthesis of Cu-based NPs an interesting and unique procedure. In our case, when TEG was used as surfactant in the presence of water as solvent (120 °C

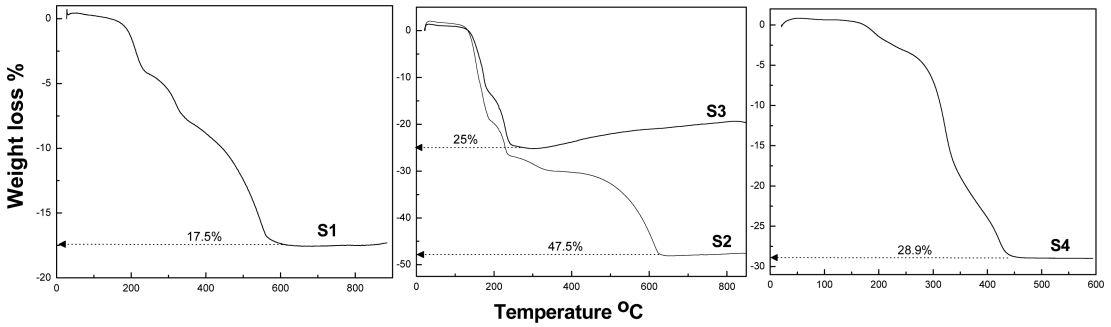

Figure 5. Thermogravimetric curves of TEG-capped (S1), OAm-capped (S2, S3) and Tween 20-capped (S4) NPs under nitrogen flow with a temperature increase of 10 C/min.

dx.doi.org/10.1021/ic501143z | Inorg. Chem. 2014, 53, 9657−9666

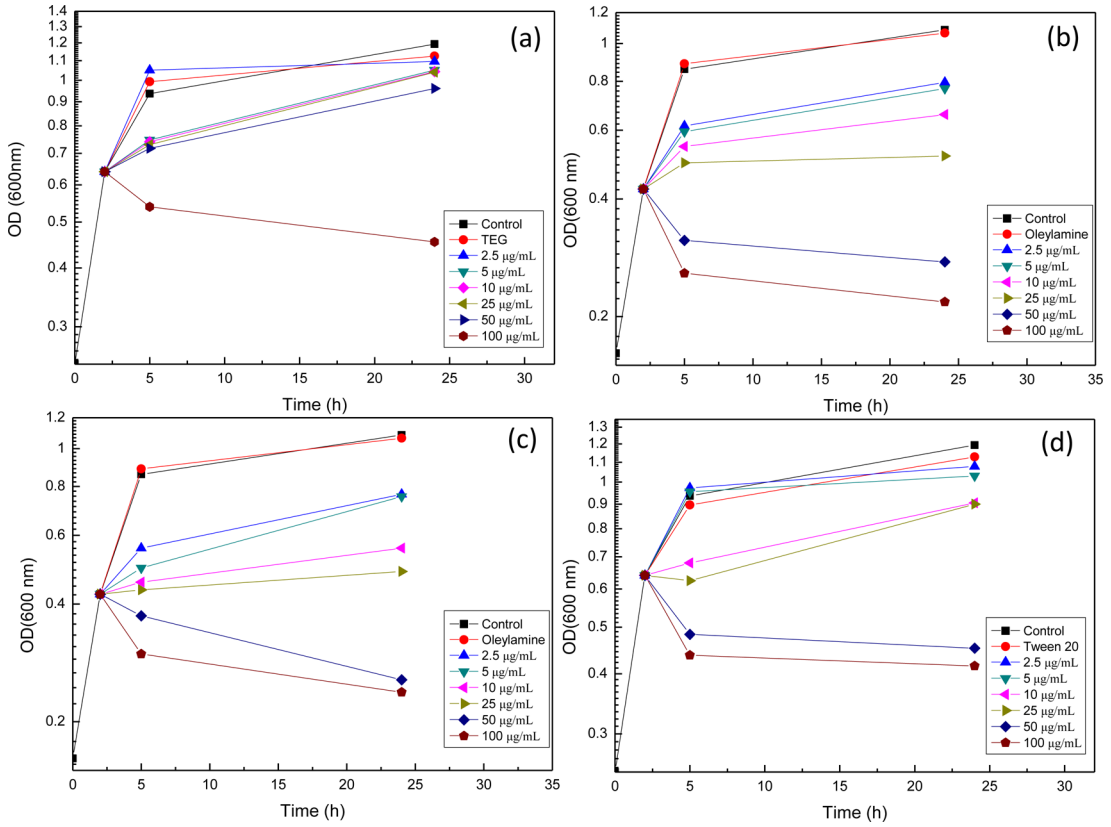

Figure 6. Antifungal activity of (a) Cu/Cu_2O@TEG NPs, (b) Cu/Cu_2O@OAm NRs, (c) Cu_2O@OAm NPs, and (d) Cu_2O@Tween 20 NPs against yeast *S. cerevisiae* cells in the presence of various concentrations of the NPs ranging from 2.5 to 100 μg/mL added at the logarithmic growth phase. Fungal growth was measured as increase in absorbance at 600 nm.

for 2 h), the polyalcohol as mild reducing agent cooperated with base and served as reduction medium for Cu^{2+} metal precursor through an intermediate Cu^{+}-TEG system mostly before transferred into the autoclave indicative of the initial brownish mixture. Afterward, disproportionation of the intermediate Cu^{+}-TEG system occurred by temperature and time, resulted to Cu nuclei as shown in reaction 2 and due to oxidative atmosphere inside the bomb, as well as the presence of NO_3^- partially surface oxidation took place and core–shell or semi shell Cu/Cu_2O NPs capped with TEG (Cu/Cu_2O@TEG) self-assembled. The small size of the NPs (7 nm) is attributed to the short time of the nucleation while TEG in the role of surfactant resulted to spherical shape. However, when TEG was used before in a double role, surfactant and solvent, in a distillation synthesis metallic rodlike Cu NPs of 36 nm were formed.[45]

$$\mathrm{Cu(NO_3)_2 + TEG + N_2H_4} \xrightarrow{\Delta} [\mathrm{Cu^{+}\cdots TEG}] \xrightarrow{\text{disproportionation}} \mathrm{Cu^0 + Cu^{2+}_{(aq)}} \quad (2)$$

The role of OAm in nanoparticle synthesis has been recently reviewed and illustrated all the important aspects in the formation of noble metal NPs, semiconductors and transition metal oxide NPs through different synthetic methods.[46] Nevertheless, OAm has not been reported until now in a solvothermal synthesis of Cu-based NPs. OAm acted as a multifunctional component in both syntheses: (i) as mild reducing agent (long-chain primary alkylamine) (ii) as complexing agent with copper ion (σ-donor) and (iii) as capping agent for stabilizing formed particles (S2 and S3). Also, it served as a solvent (S2) as it is liquid in room temperature with high boiling point (348–350 °C) that resists heating while allows a high temperature wet route to be carried out (200 °C). In both synthetic procedures, by increasing the temperature the intermediate Cu^{+}-OAm complex is formed, as previously reported.[47] Concerning sample S2, disproportionation reaction resulted to metallic Cu as shown in reaction (i) of eq 3, which due to the oxidative atmosphere (NO_3^-, air) led to heterogeneous Cu/Cu_2O architectures capped with OAm (Cu/Cu_2O@OAm). The isolated heterogeneous structure has rodlike shape that consists of 87.2% Cu_2O and 12.8% Cu. The increased concentration of OAm in this sample gave rise to σ-donor affinity; spin–orbit coupling increases as the crystal field splitting decreases and therefore favors the increment of the crystalline anisotropy of the surface layer and nanorods resulted. Interestingly these architectures are somehow similar to those reported recently[34] for Cu nanowires (50 nm) that have been formed in the presence of pure OAm by thermal decomposition in inert atmosphere, while a small ratio of Cu_2O pits was found after exposure to humid air. However, when an extra reducing agent (hydrazine) was used in proportion of water, a comproportionation reaction was favored, and the metallic Cu and Cu^{2+} resulted in Cu_2O NPs (reaction (ii) of eq 3). We assume that the nearly spherical shape of NPs derives from the nonmiscible mixture phases (OAm/H_2O) that led to reverse micelles.

dx.doi.org/10.1021/ic501143z | *Inorg. Chem.* 2014, 53, 9657–9666

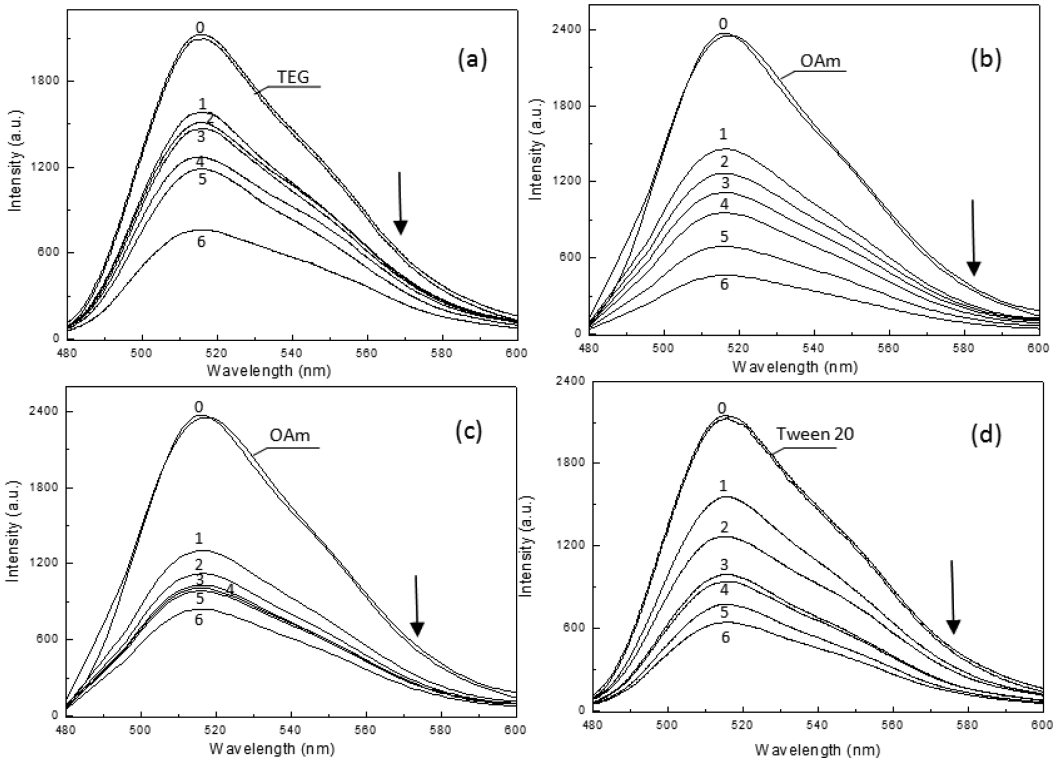

Figure 7. Viability of yeast *S. cerevisiae* cells in the presence of various concentrations of the NPs ranging from 0 to 100 μg/mL added at the logarithmic growth phase. (a) Cu/Cu_2O@TEG NPs, (b) Cu/Cu_2O@OAm NRs, (c) Cu_2O@OAm NPs and (d) Cu_2O@Tween 20 NPs. (0) stand for control, while the concentration (1)−(6) of the NPs gradually increases from 2.5 to 100 μg/mL. Fluorescence was measured at λ_{ex} = 455 nm and $\lambda_{em\ max}$ = 515 nm.

$$\left.\begin{array}{l} Cu(NO_3)_2 + OAm(i) \\ Cu(NO_3)_2 + OAm + N_2H_4(ii) \end{array}\right\} \xrightarrow{\Delta} [Cu^+ \cdots OAm]$$
$$\xrightarrow{\text{(i)disproportionation}} Cu^0 + Cu^{2+}{}_{(aq)} \xrightarrow{\text{(ii)comproportionation}} 2Cu^+ \quad (3)$$

Tween 20 is not widely used as a surfactant. However, as mentioned previously by us, initially Cu nuclei are formed and oxidize further depending on the time and temperature of the reaction.[20,21] It is worth mentioning that we received before NPs of the same composition with similar size (13 nm), although inert atmosphere in a batch reactor has been used, indicating a self-assembly organization of the defined composition (Cu_2O@Tween 20).

3.3. Antifungal Activity of NPs. The antifungal activity of the NPs (average of three measurements) toward yeast *S. cerevisiae* was estimated in terms of growth inhibition and viability by optical density and fluorescence measurements. The fluorescence method is more sensitive compared to the optical density measurement since in the latter case the turbidity is measured, and we cannot distinguish between viable and lysed cells. However, OD measurement is commonly used in antimicrobial studies and the results are considered accurate. In both experimental procedures two controls were also included: fungal cells without NPs and fungal cells with the respective organic coating of the NPs.

The time-dependent growth inhibition was determined in the presence of various concentrations of the NPs (2.5−100 μg/mL) added at the logarithmic growth phase. As seen from the growth curves in Figure 6, yeast growth inhibition is observed in a concentration-dependent manner. Meanwhile, the net mass of the fungi is affected by the NPs, as cytotoxic or lysis phenomena took place, in particular when the concentration of the NPs is high. The OD values were measured after 2 h (just before their inoculation with the NPs) were not the same for all samples, as different precultures were prepared. In detail, after 3 h of incubation the inhibition rates were more prominent (28%−70%) in the presence of increasing concentrations of Cu_2O@OAm NPs and Cu/Cu_2O@OAm NRs, while Cu_2O@Tween 20 NPs inhibited the fungal growth up to 53%. The yeast cells were relatively resistant to Cu/Cu_2O@TEG NPs, since the growth inhibition did not exceed 42%. Following 22 h of incubation, the above tendency was preserved only for the bigger concentrations, which caused further growth inhibition. In the presence of up to 25 μg/mL concentrations the fungal cells seem to develop a mechanism for overcoming the stress induced by the NPs, although their growth remains reduced compared to the control.

The fungus viability was estimated by determining the degree of esterase activity of *S. cerevisiae* cells. As a substrate we implemented fluorescein diacetate (FDA), which is enzymatically cleaved into fluorescein and acetic acid when the fungus is metabolic active. The released fluorescein was then measured by fluorescence, and the results, shown in Figure 7, demonstrate that in the controls, the highest release was promoted. However, after adding 2.5 to 100 μg/mL of the NPs to the cultures (logarithmic phase) and incubation for 3 h, the viability of the fungi is decreased in a concentration-dependent manner indicating that way that the total esterase activity is affected. It must be mentioned that as the concentration of the NPs increased, a shoulder peak at the wavelength region of 540−550 nm was recorded, attributed to the luminescence

dx.doi.org/10.1021/ic501143z | *Inorg. Chem.* 2014, 53, 9657−9666

properties of Cu_2O NPs. In general, Cu_2O NPs possess distinct luminescence properties as exhibited by a strong band at 493 nm, while the emission peak profile depends on the size and morphology of the NPs as well as to the presence of defects.[48,49]

Following 3 h of incubation with the NPs, the minimum inhibitory concentration (MIC) values (IC_{50}), which refer to either the fungal growth (optical density) or the fungal viability (fluorescence), were calculated and are summarized in Table 2.

Table 2. Antifungal Activity of the NPs Evaluated by the Half-Minimal Inhibitory Concentration (IC_{50}) (μg/mL)

samples	$IC_{50growth}$ (μg/mL) (optical density $A_{600\ nm}$)	$IC_{50viability}$ (μg/mL) (fluoresence)
Cu/Cu_2O@TEG NPs	>100	62.63
Cu/Cu_2O@OAm NRs	47.55	6
Cu_2O@OAm NPs	34.35	3.73
Cu_2O@Tween 20 NPs	56.56	7.65

Clearly, from Table 2, *S. cerevisiae* cells were more sensitive to Cu_2O NPs while the lowest IC_{50} values in terms of growth inhibition (34.35 μg/mL) and viability (3.73 μg/mL) were recorded for Cu_2O@OAm NPs. Taking into account that sizes of Cu_2O@OAm and Cu_2O@Tween 20 NPs are distinctly different (30 and 12 nm, respectively) the enhanced antifungal activity demonstrated in both cases is attributed mainly to their composition. On the other hand, the IC_{50} values calculated for the two Cu/Cu_2O NPs are remarkably different. Specifically, the yeast cells were much more sensitive to the heterogeneous Cu/Cu_2O@OAm NRs of 170 nm ($IC_{50viability}$ = 6 μg/mL) than to Cu/Cu_2O@TEG NPs of 7 nm ($IC_{50viability}$ = 62.63 μg/mL), indicating that either the big difference in their size and/or the difference in their composition (Cu/Cu_2O@TEG NPs consist of 1:1 Cu to Cu_2O phase, while Cu/Cu_2O@OAm NRs of 87.2% Cu and 12.8% Cu_2O) affected their antifungal activity; in that way *S. cerevisiae* cells showed enhanced resistance to metallic copper similar to human cells due to their common origin (eukaryotic organisms). However, by comparing the activity of all samples, we conclude that the yeast cells were sensitive both to the heterogeneous Cu/Cu_2O@OAm NRs of 170 nm and to nearly spherical Cu_2O@Tween 20 NPs of 12 nm, as indicated by the almost neighbor $IC_{50\ viability}$ values (6 and 7.25 μg/mL, respectively), demonstrating that the NPs of the same chemical composition (mainly Cu_2O) performed better against *S. cerevisiae*, even if their morphology and size differed markedly. On the basis of the above results, we suggest that the heterogeneous Cu/Cu_2O NRs affect the fungus indirectly by provoking membrane damage or ROS production, while the smaller nearly spherical NPs could also affect directly *S. cerevisiae* by influencing particle-specific biological effects. It has to be noted that ionic release was not measured due to the procedure followed, as DNA extracted from the fungal cultures treated with the NPs. However, we previously found that the released ions from Cu_2O NPs of 16 nm coated with PEG 8000 (a surfactant of similar molecular weight with Tween 20) were insufficient to provoke antimicrobial activity.[20] Moreover, NPs coated with OAm were more efficient antifungal agents, attributed to the bigger amount of OAm molecules bound on the NPs and/or the type of surfactant. As previously stated the surfactants disrupt the cell walls of the yeasts, which increases in turn their sensitivity to the NPs.[50]

3.4. DNA Binding/Degradation Experiments after Exposure to NPs in Agarose Gel Electrophoresis. The effect of the NPs on DNA isolated from *S. cerevisiae* cells treated for 22 h at 30 °C with gradually increasing concentrations of samples S1−S4 ranging from 10 to 100 μg/mL was studied. A representative electrophoretic pattern of agarose gel electrophoresis is shown in Figure 8. DNA isolated from untreated *S. cerevisiae* cells and/or from cells treated with pure surfactants (TEG, OAm, and Tween 20) exhibit one major characteristic band of unaffected/intact chromosomal DNA (Lanes 1−4: controls), while DNA isolated from cells treated with the NPs exhibit more than one bands, indicating that manner that the NPs either managed to enter the cells and come directly in contact with the DNA or ROS production and ionic release took place which affected indirectly the DNA integrity.

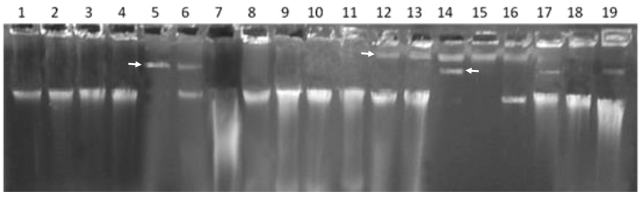

Figure 8. Dose-dependent DNA degradation action of the NPs in agarose gel electrophoresis. Lanes 1−4: control, DNA incubated in water with TEG, OAm, and Tween 20, respectively; Lanes 5−7: DNA treated with 25, 50, and 100 μg/mL of Cu_2O@Tween 20 NPs (S4); Lanes 8−11: DNA treated with 10, 25, 50, and 100 μg/mL of Cu/Cu_2O@OAm NRs (S2); Lanes 12−15:10, 25, 50, and 100 μg/mL of Cu/Cu_2O@TEG NPs (S1); Lanes 16−19: DNA treated with 10, 25, 50, and 100 μg/mL of Cu_2O@OAm NPs (S3).

DNA isolated from *S. cerevisiae* cells treated for 22 h at 30 °C with 25, 50, and 100 μg/mL of Cu_2O@Tween 20 NPs (Lanes 5−7) exhibited a higher molecular weight band (Figure 8, lanes 5 and 6) than the initial followed by disappearance of the last (Figure 8, lane 5). This outcome supports the binding effect of many NPs to DNA resulting in increase of the DNA molecular weight with concomitant delay in its electrophoretic mobility. Figure 8, lane 7 also strongly supports this suggestion where the highest concentration of NPs affected DNA integrity and resulted in significant degradation effect. A similar effect was appeared with Cu/Cu_2O@TEG NPs (Figure 8, lanes 12−15) where a DNA band of higher molecular weight was displayed with the concomitant disappearance of the main initial DNA band especially in the higher concentrations of 50 and 100 μg/mL of the NPs (Figure 8, lanes 14 and 15). Moreover, DNA isolated from *S. cerevisiae* cells treated with Cu/Cu_2O@OAm NPs showed again the formation of a high molecular weight band in the lowest concentration (Figure 8, lane 16), while in higher concentrations (Figure 8, lane 17−19) exhibited again a high molecular weight band but lower than the band in lane 16 (probably fragmented from the higher one). Additionally the DNA fragmentation starts with a concentration-dependent manner as it is reflected in the long smearing effect of the DNA tail due to DNA degradation products separated all along the gel (Figure 8, lanes 17−19). However, in case of Cu/Cu_2O@OAm NRs (170 nm) a different way of interaction is observed (Figure 8, lanes 8−11), since NRs did not manage to enter the cells and directly bind with DNA and as a result only concentration-dependent degradation effect was observed, in

dx.doi.org/10.1021/ic501143z | Inorg. Chem. 2014, 53, 9657−9666

agreement with the results that came from fungal growth inhibition and viability.

3.5. Oxidative Stress of *S. cerevisiae* Cells after Exposure to NPs. The causation of oxidative stress by the NPs was also investigated, since even if the fungal cells have rigid cell wall, its disruption by ROS may change the membrane permeability and increase the entry of NPs into the cells, while subcellular organelles may also be damaged.[19] The results demonstrate that the NPs generated oxidative stress in the *S. cerevisiae* cultures associated with the increase of O_2^- in the fungal cytoplasm (Figure 9). A significant dose-dependent

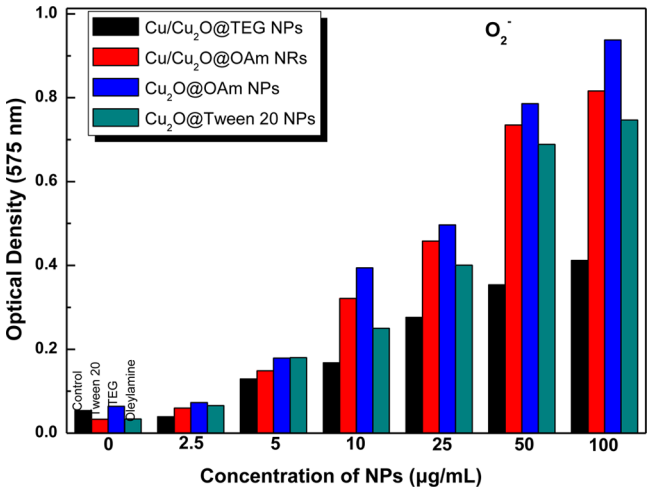

Figure 9. Intracellular O_2^- generated by Cu/Cu_2O@TEG NPs, Cu/Cu_2O@OAm NRs, Cu_2O@OAm NPs, and Cu_2O@Tween 20 NPs in *S. cerevisiae* detected by nitroblue tetrazolium assay.

response was observed in the assay for all the samples. The NBT assay is in agreement with the growth inhibition and viability measurements, since in the case of Cu_2O@OAm NPs significant stimulus was recorded, whereas in the case of Cu/Cu_2O@TEG NPs the stimulus was less pronounced. In general, low concentrations stimulated the generation of O_2^- with a moderate manner, while a maximum stimulus in higher concentration tested (100 μg/mL) was found. This result supports involvement of the oxidative stress caused by the NPs to their antifungal activity.

The membrane damage of the yeast in terms of increased porosity is exerted via lipid peroxidation, a signature of ROS damage, which can be detected by assaying for MDA, an oxidized product of polyunsaturated fatty acids. MDA forms an adduct with thiobarbituric acid (TBA), resulting in a pink product with increased absorbance at 535 nm.[30] To determine the effect of the NPs on membrane lipid peroxidation we followed the MDA production and the results showed that the MDA equivalents were gradually increased with increasing concentration of NPs from 2.5 to 100 μg/mL after 1 h of exposure (Figure 10). It is notable that the highest levels of MDA were recorded in the case of Cu_2O@OAm NPs, whereas the lowest levels were recorded in the presence of Cu/Cu_2O@TEG NPs, as we expected from the NBT results.

Consequently, it has been proved via NBT and MDA assays that the NPs (especially those of sizes >7 nm) can affect indirectly the fungus by intracellular and/or extracellular ROS production, while ions that could also be released from the NPs to promote ROS production cannot be excluded.[51] Nevertheless, at least in the case of 7 nm nearly spherical Cu/Cu_2O@

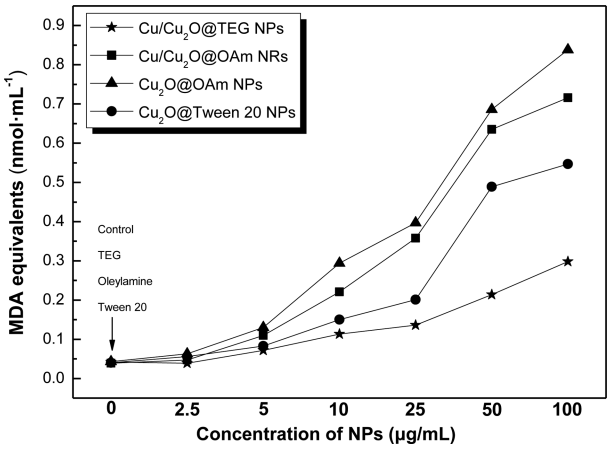

Figure 10. Increase in the MDA equivalents (nmol/mL) compared to the control batch (i.e., without NPs in culture media) after 1 h of exposition with 2.5−100 μg/mL of Cu/Cu_2O@TEG NPs, Cu/Cu_2O@OAm NRs, Cu_2O@OAm NPs, and Cu_2O@Tween 20 NPs. The results correspond to mean ± SD (SD, standard deviation; n = 3).

TEG NPs the nanosized effect is predominant, as ROS amounts were found to be of a low level.

4. CONCLUSIONS

Selective solvothermal synthesis of Cu_2O and heterogeneous Cu/Cu_2O NPs of different sizes and shapes was mainly driven by surfactants. The newly prepared nanostructures, explored herein for biological properties, are important also for their applications in electronics, optics, and catalysis. Their enhanced antifungal activity, demonstrated in this paper, makes us optimistic for their use as antimicrobial agents and renders them a compelling alternative to the microbial resistance problem. Their mechanism of action was investigated, and DNA interaction in terms of binding and degradation has been proved, while ROS production and lipid peroxidation have been verified. However, further studies with NPs within a range of sizes and shapes need to be done to establish their activity pathway.

AUTHOR INFORMATION

Corresponding Author

*E-mail: samkat@chem.auth.gr.

Notes

The authors declare no competing financial interest.

ACKNOWLEDGMENTS

The authors C.D.-S. and K.G. are grateful for the financial support of the European Union (European Social Fund (ESF)) and Greek national funds through the Operational Program "Education and Lifelong Learning" of the National Strategic Reference Framework (NSRF)—Research Funding Program: Thales.

REFERENCES

(1) Huang, A. W. R.; Covell, D. G. *Biochem. Pharmacol.* **2005**, *69*, 1009−1039.

(2) Kim, K.-J.; Sung, W. S.; Suh, B. K.; Moon, S. K.; Choi, J.-S.; Kim, J. G.; Lee, D. G. *Biometals* **2009**, *22*, 235−242.

(3) Li, Q. L.; Mahendra, S.; Lyon, D. Y.; Brunet, L.; Liga, M. V.; Li, D.; Alvarez, P. J. J. *Water Res.* **2008**, *42*, 4591−4602.

(4) Ansari, A. A.; Khan, M. N.; Alhoshan, M.; Aldwayyan, A. S.; Alsalhi, M. S. In *Nanoparticles;* Kestell, A. E., DeLorey, G. T., Eds.; Nova Science Publishers, Inc.: Hauppauge, NY, 2010, 1−78.
(5) *Metallic Nanomaterials;* Kumar, C. S. S. R., Ed.; Wiley-VCH Verlag GmbH & Co KGaA: Weinheim, Germany, 2009.
(6) Usman, M. S.; Zowalaty, M. E. E.; Shameli, K.; Zainuddin, N.; Salama, M.; Ibrahim, N. A. *Int. J. Nanomed.* **2013**, *8*, 4467−4479.
(7) Applerot, G.; Lellouche, J.; Lipovsky, A.; Nitzan, Y.; Lubart, R.; Gedanken, A.; Banin, E. *Small* **2012**, *8*, 3326−3337.
(8) Chatterjee, A. K.; Sarkar, R. K.; Chattopadhyay, A. P.; Aich, P.; Chakraborty, R.; Basu, T. *Nanotechnology* **2012**, *23*, 085103 DOI: 10.1088/0957-4484/23/8/085103.
(9) Ramyadevi, J.; Jeyasubramanian, K.; Marikani, A.; Rajakumar, G.; Rahuman, A. A. *Mater. Lett.* **2012**, *71*, 114−116.
(10) Azam, A.; Ahmed, A. S.; Oves, M.; Khan, M. S.; Memic, A. *Int. J. Nanomed.* **2012**, *7*, 3527−3535.
(11) Baek, Y.-W.; An, Y.- J. *Sci. Total Environ.* **2011**, *409*, 1603−1608.
(12) Vellora, V.; Padil, T.; Černík, M. *Int. J. Nanomed.* **2013**, *8*, 889−898.
(13) Karlsson, H. L.; Gustafsson, J.; Cronholm, P.; Muller, L. *Toxicol. Lett.* **2009**, *188*, 112−118.
(14) Gopalakrishnan, K.; Ramesh, C.; Ragunathan, V.; Thamilselvan, M. *Dig. J. Nanomater. Bios.* **2012**, *7*, 833−839.
(15) Pang, H.; Gao, F.; Lu, Q. *Chem. Commun.* **2009**, 1076−1078.
(16) Ren, J.; Wang, W.; Sun, S.; Zhang, L.; Wang, L.; Chang, J. *Ind. Eng. Chem. Res.* **2011**, *50*, 10366−10369.
(17) Wei, Y.; Chen, S.; Kowalczyk, B.; Huda, S.; Gray, T. P.; Grzybowski, B. A. *J. Phys. Chem. C* **2010**, *114*, 612−616.
(18) Kanhed, P.; Birla, S.; Gaikwad, S.; Gade, A.; Seabra, A. B.; Rubilar, O.; Duran, N.; Rai, M. *Mater. Lett.* **2014**, *115*, 13−17.
(19) Kasemets, K.; Ivask, A.; Dubourguier, H.-C.; Kahru, A. *Toxicol. In Vitro* **2009**, *23*, 1116−1122.
(20) Giannousi, K.; Lafazanis, K.; Arvanitidis, J.; Pantazaki, A.; Dendrinou-Samara, C. *J. Inorg. Biochem.* **2014**, *133*, 24−32.
(21) Giannousi, K.; Avramidis, I.; Dendrinou-Samara, C. *RSC Adv.* **2013**, *3*, 21743−21752.
(22) Nomura, T.; Miyazaki, J.; Miyamoto, A.; Kuriyama, Y.; Tokumoto, H.; Konishi, Y. *Environ. Sci. Technol.* **2013**, *47*, 3417−3423.
(23) Suresh, A. K.; Pelletier, D. A.; Doktycz, M. J. *Nanoscale* **2013**, *5*, 463−474.
(24) Tsiaggali, M. A.; Andreadou, E. G.; Hatzidimitriou, A. G.; Pantazaki, A. A.; Aslanidis, P. *J. Inorg. Biochem.* **2013**, *121*, 121−128.
(25) Williams, D. N.; Ehrman, S. H.; Holoman, T. R. P. *J. Nanobiotechnol.* **2006**, *4*, 3.
(26) Verma, P.; Dyckmans, J.; Militz, H.; Mai, C. *Appl. Microbiol. Biotechnol.* **2008**, *80*, 125−133.
(27) Harju, S.; Fedosyuk, H.; Peterson, K. R. *BMC Biotechnol.* **2004**, 4 DOI: 10.1186/1472-6750-4-8.
(28) Herrmann, M.; Lorenz, H. M.; Voll, R.; Grunke, M.; Woith, W.; Kalden, J. R. *Nucleic Acids Res.* **1994**, *22*, 5506−5507.
(29) Becerra, M. C.; Eraso, A. J.; Albesa, I. *Luminescence* **2003**, *18*, 334−340.
(30) Dutta, R. K.; Nenavathu, B. P.; Gangishetty, M. K.; Reddy, A. V. R. *Colloids Surf., B* **2012**, *94*, 143−150.
(31) Feris, K.; Otto, C.; Tinker, J.; Wingett, D.; Punnoose, A.; Thurber, A.; Kongara, M.; Sabetian, M.; Quinn, B.; Hanna, C.; Pink, D. *Langmuir* **2010**, *26*, 4429−4436.
(32) Jeong, S.; Song, H. C.; Lee, W. W.; Lee, S. S.; Choi, Y.; Son, W.; Kim, E. D.; Paik, C. H.; Oh, S. H.; Ryu, B. H. *Langmuir* **2011**, *27*, 3144−3149.
(33) Son, S. U.; Park, I. K.; Park, J.; Hyeon, T. *Chem. Commun.* **2004**, 778−779.
(34) Ye, E.; Zhang, S.-Y.; Liu, S.; Han, M.-Y. *Chem.—Eur. J.* **2011**, *17*, 3074−3077.
(35) Yusuf, S. M.; De Teresa, J. M.; Mukadam, M. D.; Kohlbrecher, J.; Ibarra, M. R.; Arbiol, J.; Sharma, P.; Kulshreshtha, S. K. *Phys. Rev. B* **2006**, *74*, 224428−11.
(36) Dendrinou-Samara, C.; Psomas, G.; Raptopoulou, C. P.; Kessissoglou, D. P. *J. Inorg. Biochem.* **2007**, *83*, 7−16.
(37) Zhang, Y. C.; Tang, J. Y.; Wang, G. L.; Zhang, M.; Hu, X. Y. *J. Cryst. Growth* **2006**, *294*, 278−282.
(38) Debbichi, L.; Marco de Lucas, M. C.; Pierson, J. F.; Krüger, P. *J. Phys. Chem. C* **2012**, *116*, 10232−10237.
(39) Shinde, S. L.; Nanda, K. K. *RSC Adv.* **2012**, *2*, 3647−3650.
(40) Hassanien, R. S. A.; Farha, Al-Said; Siller, L.; Little, R.; Wright, N. G.; Houlton, A.; Horrocks, B. R. *Nanotechnol.* **2012**, *23*, 1−12.
(41) Bastami, T. R.; Entezari, M. H.; Hua, Q. H.; Hartono, S. B.; Qia, S. Z. *Chem. Eng. J.* **2012**, *210*, 157−165.
(42) Shen, L.; Laibinis, P. E.; Hatton, T. A. *Langmuir* **1999**, *15*, 447−453.
(43) Si, S.; Kotal, A.; Mandal, T. K.; Giri, S.; Nakamura, H.; Kohara, T. *Chem. Mater.* **2004**, *16*, 3489−3496.
(44) De Palma, R.; Peeters, S.; Van Bael, M. J.; Van den Rul, H.; Bonroy, K.; Laureyn, W.; Mullens, J.; Borghs, G.; Maes, G. *Chem. Mater.* **2007**, *19*, 1821−1831.
(45) Carroll, K. J.; Reveles, J. U.; Shultz, M. D.; Khanna, S. N.; Carpenter, E. E. *J. Phys. Chem. C* **2011**, *115*, 2656−2664.
(46) Yang, H.-J.; He, S.-Y.; Tuan, H.-Y. *Langmuir* **2014**, *30*, 602−610.
(47) Mourdikoudis, S.; Liz-Marzán, L. M. *Chem. Mater.* **2013**, *25*, 1465−1476.
(48) Yang, Z.; Chiang, C.-K.; Chang, H.-T. *Nanotechnology* **2008**, 19 DOI: 10.1088/0957-4484/19/02/025604.
(49) Sharma, P.; Bhatti, H. S. *Mater. Chem. Phys.* **2009**, *114*, 889−896.
(50) Panacek, A.; Kolar, M.; Vecerova, R.; Prucek, R.; Soukupova, J.; Krystof, V.; Hamal, P.; Zboril, R.; Kvıtek, L. *Biomaterials* **2009**, *30*, 6333−6340.
(51) Chang, Y.-N.; Zhang, M.; Xia, L.; Zhang, J.; Xing, G. *Materials* **2012**, *5*, 2859−2871.